Int. J. Electrochem. Sci., 8 **(2013)** 3928 - 3938

International Journal of
ELECTROCHEMICAL
SCIENCE
www.electrochemsci.org

Preparation and Characterization of Novel Sandwich-Typed Three-Dimensional Bimodal Nanoporous Copper-Supported Tin Thin-Film Anode for Lithium Ion Battery

Wenbo Liu[1,2,*], *Shichao Zhang*[1,*], *Ning Li*[2], *Shenshen An*[1] *and Jiwei Zheng*[1]

[1] School of Materials Science and Engineering, Beihang University, Beijing 100191, China
[2] School of Manufacturing Science and Engineering, Sichuan University, Chengdu 610065, China
[*]E-mail: liuwenbo_8338@163.com; csc@buaa.edu.cn

Received: 20 November 2012 / *Accepted:* 23 January 2013 / *Published:* 1 March 2013

We reported a unique sandwich-typed three-dimensional bimodal nanoporous copper-supported tin (3D-BNPC/Sn) thin-film anode for lithium-ion batteries (LIBs) prepared by partly chemical dealloying of as-cast Al 15 at.% Cu alloy slices followed by electroless depositing of a thin layer of tin in an alkaline solution. The microstructure of the 3D-BNPC/Sn thin-film electrode was characterized using X-ray diffraction, scanning electron microscopy, energy dispersive X-ray analysis, and its electrochemical performance was investigated by galvanostatic charge/discharge cycling test. The results show that the 3D-BNPC/Sn thin-film anode exhibits much higher first discharge capacity and better initial Coulombic efficiency than that of two-dimensional (2D) counterpart, which can be attributed to the special 3D bimodal porous structure and large active surface area, suggesting that the 3D-BNPC/Sn thin-film anode possesses a promising application in high-performance LIBs.

Keywords: Lithium ion battery; Dealloying; Porous structure; Bimodal; Tin anode

1. INTRODUCTION

Although widely used in the field of various portable electric devices as a power supply, lithium ion batteries still have attracted much attention in attempts to ameliorate the performance of their inside components. As a successful application in lithium-ion batteries, carbonaceous materials have many advantages such as stable charge-discharge properties and low-cost [1]. However, since their theoretical capacity is only 372 mAh g^{-1} for LiC_6, it is great important to develop new anode materials with higher capacity for LIBs. Compared with graphite, Sn and Li can form $Li_{4.4}Sn$ in lithiation process with theoretical capacity of 994 mAh g^{-1}, which has attracted researchers' great interest [2]. Unfortunately, such material is known to suffer from dramatic severe volume change

(expansion and contraction over 200%) during lithiation/delithiation process, which leads to pulverization and poor cycle life, and thus severely inhibited its application in LIBs [3-8].

The current strategies to overcome the pulverization of tin mainly include reducing the size of active material to nano-scale [9-11], using active/inactive composite as strain buffer [4,12-13], and adopting 3D current collector [14,15]. Nanostructured material have unique advantages in mass transport which leads to easy diffusion of electron and ion, higher electrode/electrolyte interfacial contact area and better accommodation of structural strain during lithiation/delithiation reactions [16]. Simon et al. [17] reported a nano-architectured electrode by depositing tin on copper nanopillars, which exhibits good cycle performance. Moreover, in order to alleviate the severe volume change during cycling, some researchers dispersed tin into inactive components to form the active/inactive composite system and strengthen the interfacial binding force, such as Sn-Cu, Sn-Ni, Sn-Co, Sn-Mo, Sn-C, and so forth [18-23]. Tamura's study showed that the capacity retention after 10 cycles was improved from 20% to 94% due to the formation of Cu_6Sn_5 intermetallic layers between copper and tin layers by heat treatment, which enhanced the interface strength [24]. Although two- and multi-component alloys can improve the cyclability for LIBs, they still are far from commercialization. Besides, in order to further enhance the cyclability of active materials with high theoretical capacity, 3D substrates were employed as candidates of current collectors, such as carbon paper, nickel foam, copper foam, and copper cellular architecture [16,25-28]. Compared to the compact one, the foamy metals possess several prominent advantages. Firstly, it offers a good conductive environment for active materials. Moreover, its stress absorbability is beneficial to construct a stretch electrode system, which would insure good combination between active materials and substrate so that preventing the electrode failure during cycling [29].

3D nanoporous metals (NPMs) prepared by dealloying, as novel functional materials, have recently attracted considerable interest in a wide variety of technological applications including catalysis, sensors, actuators, fuel cells, microfluidic flow controllers, and so forth [30-33]. Dealloying is a special corrosion process during which the less noble atoms is selectively dissolved from alloy, leaving behind the noble metal atoms that diffused along alloy/solution interfaces and agglomerated into the porous network [34]. In the previous work, many NPMs with complicated porous structures had been successfully fabricated through some facile approaches on a basis of understanding of physical nature of dealloying and their formation mechanisms were revealed in detail [35-54]. Though NPMs have shown many achievements, as one of the most promising application fields of NPMs, few researches have so far conducted in LIBs.

In this article, we propose a strategy to prepare a unique sandwich-typed 3D bimodal nanoporous copper-supported tin thin-film anode for LIBs by electroless plating a thin layer of tin onto sandwich-typed bimodal NPC (which serves as both the current collector and substrate of active materials). The unique 3D BNPC is fabricated by partly chemical dealloying of as-cast Al 15 at.% Cu alloy slices in an acidic solution. The obtained 3D-BNPC/Sn thin-film anode, as an active/inactive composite, could take advantage of nanoporous structure for better mass transport and larger active surface area. Thus, the improved electrochemical performance can be obtained and the probable mechanism is discussed. This unique nano-architectured electrode exhibits a promising application in high-performance LIBs.

2. EXPERIMENTAL SECTION

2.1. Preparation and characterization of the sandwich-typed 3D BNPC/Sn thin-film anode

Al-Cu alloy with nominal composition of 15 at.% Cu was prepared from pure Al (99.9 wt.%) and pure Cu (99.999 wt.%). Voltaic arc heating was employed to melt the charges in a copper crucible under an argon atmosphere, and then the melt was cooled down into ingots in situ. Subsequently, the alloy ingots were processed into slices by wire-cutting EDM with the thickness of about 300 μm. Prior to further treatment, the slices were washed and polished to remove oil and oxides formed on the surface. The dealloying of Al 15 at.% Cu alloy was performed in 5 wt.% HCl aqueous solution at 90℃ for different times. After dealloying, the samples were rinsed with distilled water and dehydrated alcohol for several times. The sandwich-typed 3D BNPC slices were obtained after dried in a vacuum oven at 60℃ for 48 h. To prepare the 3D-BNPC/Sn thin-film anode, electroless plating of tin was typically conducted in a plating bath containing 0.33M $SnSO_4$, 3.85M NaOH, 0.9M NaH_2PO_2 and 0.66M sodium citrate at 75℃ for 0.5 min. For comparison, 2D tin thin-film anode (2D-TTA) was also prepared by electroless plating tin onto 2D flat copper foil under the similar conditions.

Microstructural characterization and analysis of sandwich-typed BNPC and 3D-BNPC/Sn samples were made using X-ray diffraction (XRD, Rigaku D/Max-2400) with Cu Kα radiation, scanning electron microscopy (FESEM, Hitachi S-4800) with an energy dispersive X-ray (EDX) analyzer.

2.2. Cell assemble and electrochemical measurements

Electrochemical charge-discharge behaviors were investigated in simulant cells assembled with the as-prepared anode, lithium foil and Celgard 2300 membrane in an Ar-filled glove box (MB-10-G with TP170b/mono, MBRAUN). Electrolyte was 1M $LiPF_6$ in a mixed solution of EC and DEC (1:1 by v/v). Each cell was aged for 24 h at room temperature before commencing the electrochemical tests. The galvanostatic charge-discharge measurements were carried out in a battery test system (NEWARE BTS-610, Newware Technology Co., Ltd., China) for a cut-off potential of 0.01-1.5V (vs. Li/Li^+) at ambient temperature.

3. RESULTS AND DISCUSSION

Figure 1 shows the microstructure of as-dealloyed samples by chemical dealloying of as-cast Al 15 at.% Cu alloy slices in the 5 wt.% HCl solution at 90℃ for different times. For the samples by dealloying for 1 min, a thin layer of quasi-uniform bimodal porous structure can be formed on the outmost surface of the initial Al-Cu alloy, indicating the evolution of porous structure is occurring at this stage.

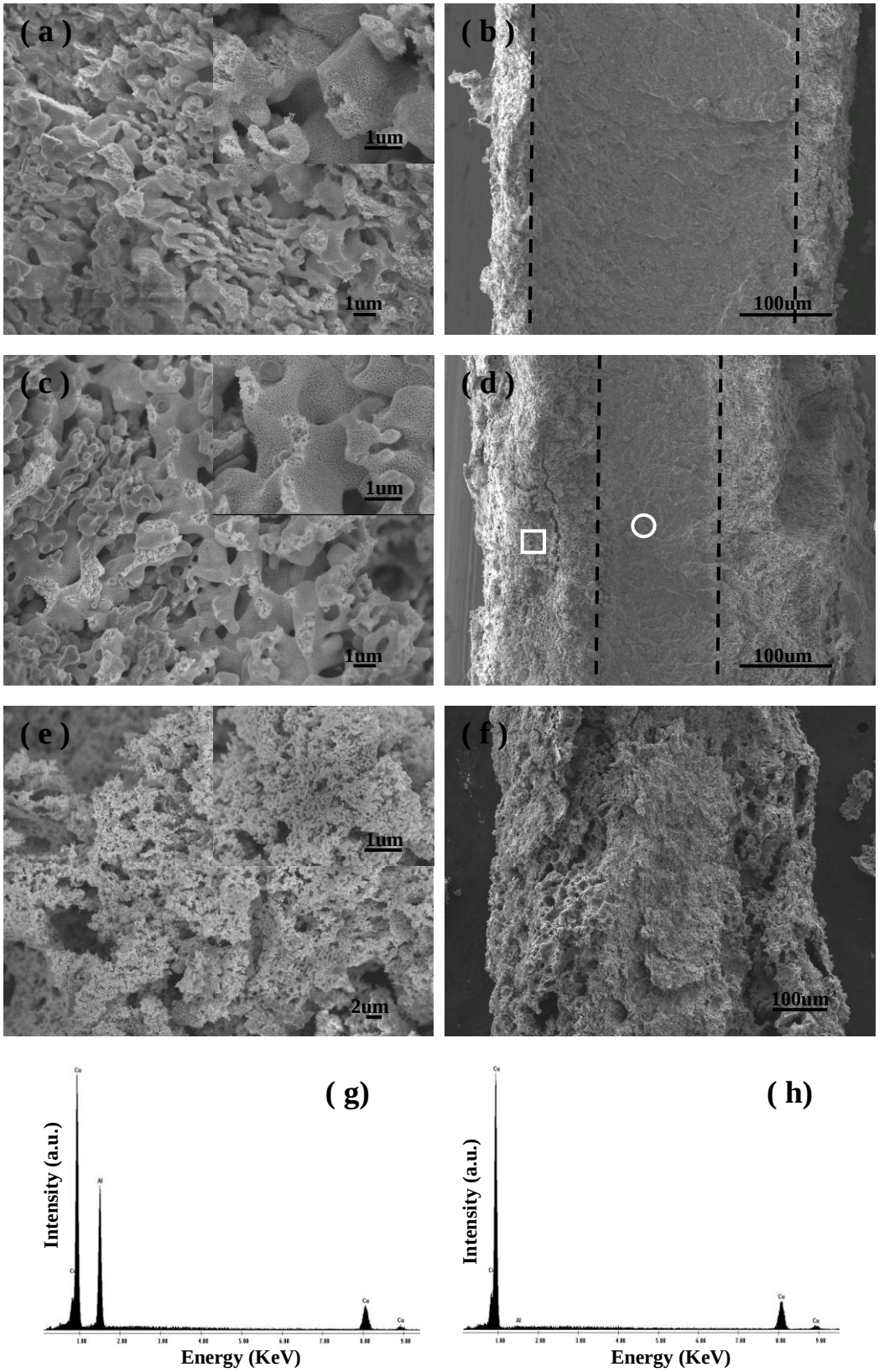

Figure 1. SEM images of as-dealloyed samples by chemical dealloying of as-cast Al 15 at.% Cu alloy slices in the 5 wt.% HCl solution at 90℃ for (a-b) 1 min, (c-d) 3 min, (e-f) 10 min. Parts a, c and e are the plane views; parts b, d and f are the section views, in which broken line denotes the boundary between porous structure and alloy layer. (g-h) EDX spectra of porous structure and alloy layer in samples marked by circle and square in part d. a.u.: arbitrary units.

When the dealloying time reaches 3 min, the surface layer of as-dealloyed samples exhibits a typical bimodal ligament-pore structure, which is composed of interconnected large-sized pores (several microns) with highly porous pore walls (tens of nm). Both large- and small-sized pores are 3D, open, and bicontinuous.

From the low-magnification section-view image of samples, we note that the thickness of porous structure layer is remarkably increased and a typical sandwich-typed microstructure comprising alternating porous structure layer and alloy layer (~ 1:1 by thickness) can be obtained. With the dealloying time keeping increasing, the porous structure layer gradually coarsens due to the Ostwald ripening effects [55], and no obvious alloy layer can be observed until the dealloying time up to 10 min. EDX analysis has been performed on the sandwich-typed 3D BNPC slices upon dealloying for 3 min, and typical spectra are shown in Figure 1g-h. It is obvious that the alloy layer is enriched in Al, and the atomic percentage of Al to Cu in the alloy layer is close to 5:1, while nearly all of Al is removed in the porous structure layer during dealloying. The present result demonstrates that the bilateral porous structure is Cu phase, and the central layer is the original Al-Cu alloy.

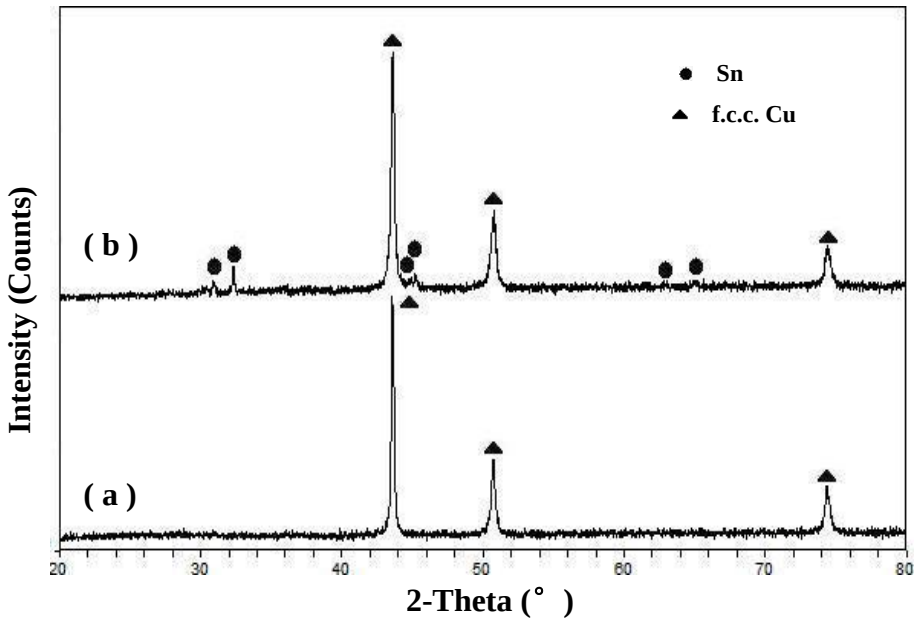

Figure 2. XRD patterns of (a) the 3D BNPC current collector by chemical dealloying of Al 15 at.% Cu alloy slices in the 5 wt.% HCl solution at 90℃ for 3 min and (b) the 3D-BNPC/Sn thin-film anode after electroless plating tin at 75℃ for 0.5 min.

In order to take advantages of merits of the special 3D porous structure (e.g. large-sized pores facilitating solvent diffusion and small-sized one contributing to enlarging active surface area), the sandwich-typed 3D BNPC slices upon dealloying in the 5 wt.% HCl solution at 90℃ for 3 min were chosen as typical current collectors and substrates of active materials herein. Figure 2 shows the XRD patterns of the 3D BNPC current collector and the 3D-BNPC/Sn thin-film anode upon electroless plating tin for 0.5 min, respectively.

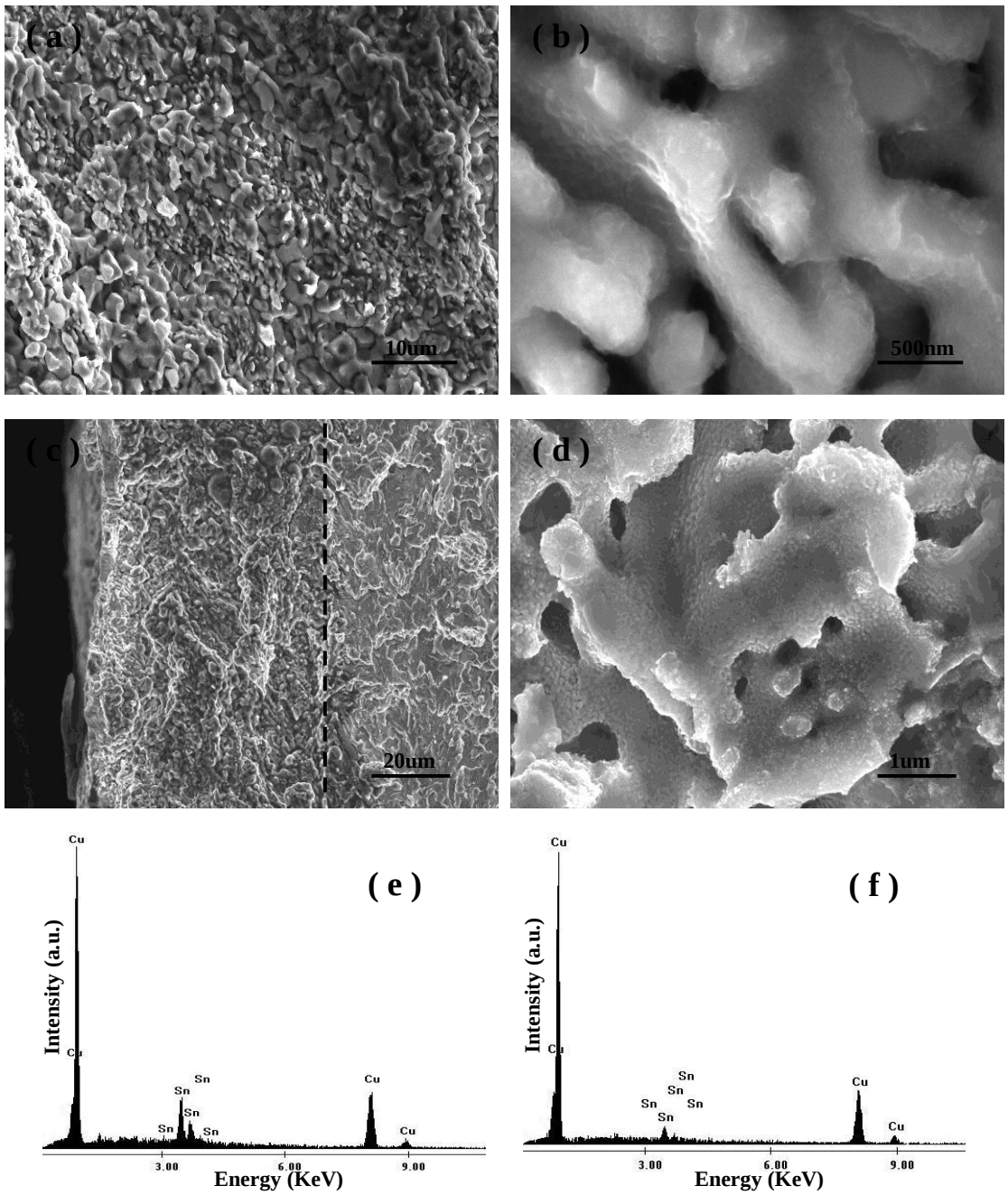

Figure 3. SEM images of sandwich-typed 3D BNPC/Sn thin-film anode by electroless plating tin on the 3D BNPC current collector in the alkaline solution at 75℃ for 0.5 min. Parts a and b are the plane views; parts c and d are the section views, in which broken line denotes the boundary between porous structure and alloy layer. (e-f) EDX spectra of porous structures corresponding to parts b and d. a.u.: arbitrary units.

The filled circles and triangles stand for Sn and Cu, respectively. As can be seen from Figure 2a, only a face-centered cubic (f.c.c.) Cu phase can be identified in the 3D BNPC current collector under the X-ray detection limit. After electroless plating, the XRD result of the 3D-BNPC/Sn thin-film anode indicates the presence of two basic phases: the minor deposited product tetragonal β-Sn and

original f.c.c. Cu substrate. It clearly demonstrates that tin as active material has been successfully deposited onto the 3D BNPC substrate upon electroless plating tin for 0.5 min.

Figure 3 shows the plane- and section-view SEM images of sandwich-typed 3D BNPC/Sn thin-film anode by electroless plating tin on the 3D BNPC current collector in the alkaline solution for 0.5 min. It is clear that a uniform and smooth layer of tin covers the surface and interior of porous structure of the 3D current collector, and the open, 3D interpenetrating bimodal porous network morphology can be well preserved in the resultant electrode after electroless plating.

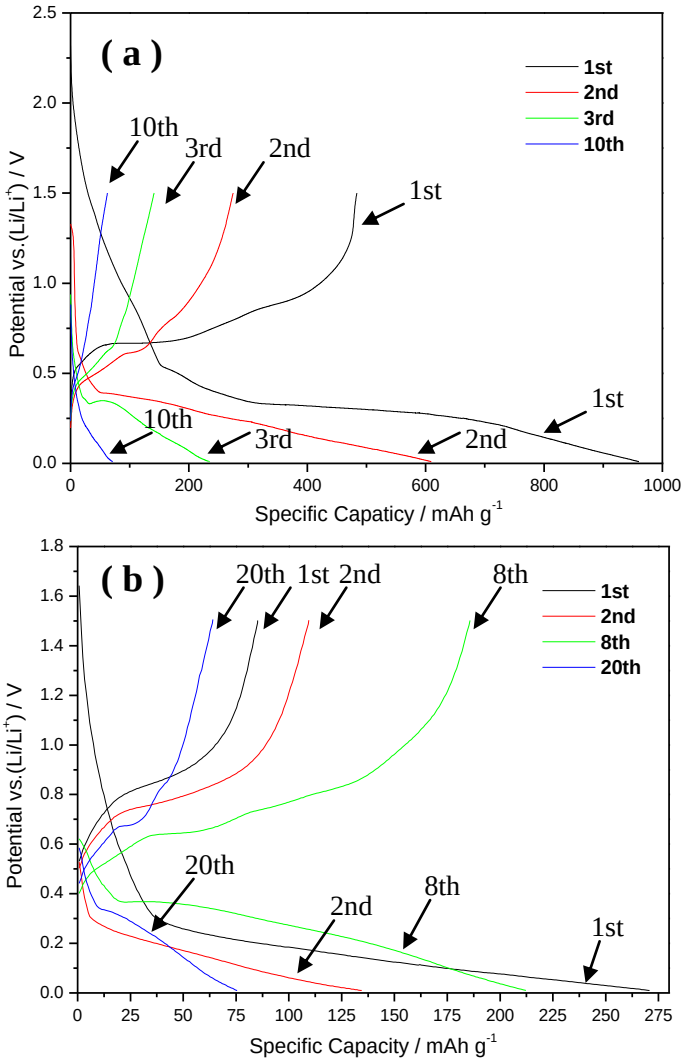

Figure 4. Charge-discharge curves of (a) the 3D-BNPC/Sn thin-film anode and (b) the 2D-TTA at 0.1C rate between 1.5V and 0.01V.

Additionally, EDX analysis has been performed on the 3D BNPC/Sn thin-film anode, and typical spectra are shown in Figure 3e-f. Obviously, both the surface and interior of the 3D porous electrode are enriched in Sn, confirming tin layer has been well deposited on the ligaments of the 3D porous substrate after electroless plating.

The charge-discharge curves of sandwich-typed 3D BNPC/Sn thin-film anode at the 0.1C rate between 1.5V and 0.01V (Figure 4a) show an efficiency of 50% during the first cycle with 960 mAh g^{-1} initial discharge capacity. It is mainly assigned to the compact microstructure of tin film which severely hinders the delithiation process and the formation of a solid electrolyte interphase (SEI) layer due to decomposition of electrolyte on the tin surface [56,57]. According to the first discharge of 3D thin-film anode, two plateaus around 0.25V and 0.5V can be clearly identified, which can be ascribed to lithium insertion into different Li_xSn phases [2,58-59]. During the charge, the 3D thin-film anode shows a slope ranging from 0.6V to 1.0V, corresponding to reversible delithiation from Li-Sn alloy. In contrast, Figure 4b shows the charge-discharge curves of the 2D-TTA that tested at the 0.1C rate between 1.5V and 0.01V. The first discharge curve of 2D-TTA exhibits Li intercalation plateaus at around 0.2V, and the initial discharge capacity is just 270 mAh g^{-1} with 31% Coulombic efficiency, about 1/4 of that of 3D BNPC/Sn thin-film anode. Therefore, compared to the 2D-TTA, the much higher first discharge capacity and better initial Coulombic efficiency can be obtained in the 3D BNPC/Sn thin-film electrode.

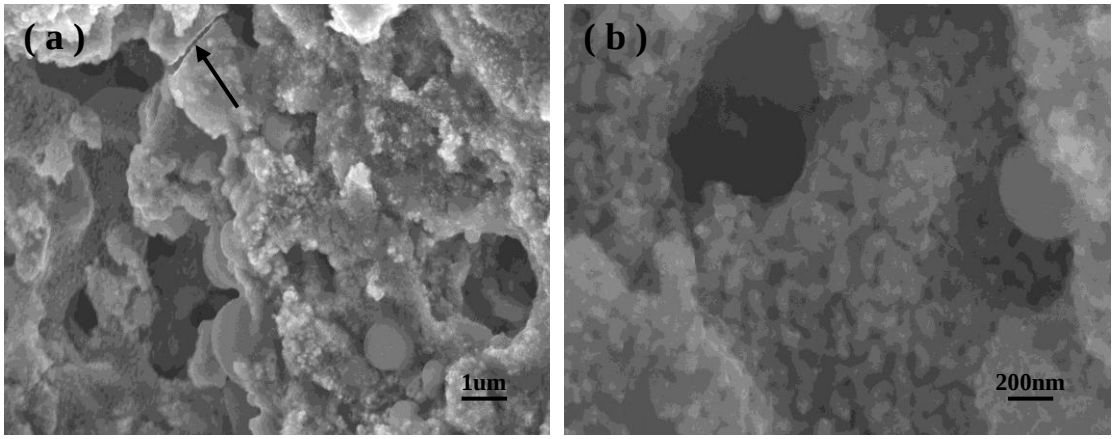

Figure 5. SEM images of the 3D-BNPC/Sn thin-film electrode after several cycles.

The improved performance of the 3D BNPC/Sn thin-film anode can be attributed to the special 3D nanoporosity design of the electrode developed from dealloying, which simultaneously contains both large- and small-sized pores. On one hand, the large-sized pores could facilitate the solvent diffusion and mass transportation while the 3D copper frame effectively functions as electron collector. On the other hand, the small-sized pores on the pore walls can also contribute greatly to enlarge the surface area and accommodate more tin with less thickness. The large specific surface area enables higher active area during reaction and thus brings better capacity. The small thickness of tin layer relieves the mechanical stress associated with huge volume expansion during cycling.

To further understand the failure mechanism of 3D BNPC/Sn thin-film electrode, SEM micrographs of the 3D thin-film anode after several galvanostatical charge-discharge cycles were shown in Figure 5. It clearly shows that the 3D porosity of the BNPC/Sn thin-film electrode is subjected to severe damage and some cracking can be observed after several cycles, implying the

sandwich-typed BNPC substrate possesses poor structural stability. Moreover, the volume expansion during discharging might cause shutdown of the connecting windows between nanopores, and thus, would isolate the active material from the electrolyte and hinder the electrochemical lithiation reaction inside the porous electrode [60]. Probably, this shutdown would lead to a decrease in the utilization of active material. It should be noted that, however, the repeated lithiation/delithiation process cannot cause obvious pulverization and shedding of tin from the 3D substrate during cycling as shown in the high-magnification SEM image (Figure 5b), indicative of a good binding force between active material and substrate.

This is the first time to report that the sandwich-typed bimodal nanoporous copper was utilized in LIBs. It may be believable that one can employ this simple and effective strategy to obtain other sandwich-typed 3D bimodal nanoporous metal-supported thin-film electrodes with large surface area and satisfactory electrochemical performance for LIBs. The performance could be further improved with the optimization of nanoporosity and structural stability of the 3D electrode.

4. CONCLUSION

In summary, a novel sandwich-typed three-dimensional bimodal nanoporous copper-supported tin thin-film anode has been prepared by partly chemical dealloying of as-cast Al 15 at.% Cu alloy slices followed by electroless depositing of a thin layer of tin in an alkaline solution. Its application in the lithium-ion battery demonstrates that the unique 3D nanoporous electrode with bimodal pore size distributions and large surface area can be a promising strategy to prepare high performance anodes. It exhibits 960 mAh g^{-1} initial discharge capacity and 50% initial Coulombic efficiency, much better than those of the 2D-TTA, which can be ascribed to the special bimodal porosity and large active surface area, indicative of a potential application in LIBs.

ACKNOWLEDGEMENT
We give thanks to financial support by the State Key Basic Research Program of PRC (2013CB934000, 2007CB936502), the National Natural Science Foundation of China (51274017, 50954005, 51074011), the National 863 Program Project (2008AA03Z208, 2011AA11A257), the China Postdoctoral Science Foundation Funded Project (2011M500214), the Basic Research Fund Project of Beihang University (501LJJC2012101001, 501LKGY2012101004), and the Shanghai Aerospace Science and Technology Innovation Fund Project (SAST201269). Also, we are grateful to Prof. T. Zhang and Dr. J.F. Wang for assistance in preparation of the Al-Cu alloy ingots.

References

1. M. Winter and R. J. Brodd, *Chem. Rev.*, 104 (2004) 4245.
2. M. Winter and J. O. Besenhard, *Electrochim. Acta*, 45 (1999) 31.
3. G. X.Wang, J. H. Ahn, J. Yao, S. Bewlay and H. K. Liu, *Electrochem. Commun.*, 6 (2004) 689.
4. K. D. Kepler, J. T. Vaughey and M. M. Thackeray, *J. Power Sources*, 81-82 (1999) 383.
5. A. H. Whitehead, J. M. Elliott and J. R. Owen, *J. Power Sources*, 81-82 (1999) 33.

6. J. Yang, M. Wachtler, M. Winter and J. O. Besenhard, *Electrochem. Solid-State Lett.*, 2 (1999) 161.
7. H. Li, X. J. Huang, L. Q. Chen, Z. G.Wu and Y. Liang, *Electrochem. Solid-State Lett.*, 2 (1999) 547.
8. Z. P. Guo, J. Z. Wang, H. K. Liu and S. X. Dou, *J. Power Sources*, 146 (2005) 448.
9. M. Valvo, U. Lafont, D. Munao and E. M. Kelder, *J. Power Sources*, 189 (2009) 297.
10. W. Choi, J. Y. Lee, B. H. Jung and H. S. Lim, *J. Power Sources*, 136 (2004) 154.
11. Y. Hu, Y. Guo, W. Sigle, S. Hore, P. Balaya and J. Maier, *Nat. Mater.*, 5 (2006) 713.
12. O. Mao, R. L. Turner, I. A. Courtney, B. D. Fredericksen, M. I. Buckett, L. J. Krause and J. R. Dahn, *Electrochem. Solid-State Lett.*, 2 (1999) 3.
13. A. Trifonova, M. Wachtler, M. R. Wagner, H. Schriettner, C. Mitterbauer, F. Hofer, K. C. Möller, M. Winter and J. O. Besenhard, *Solid State Ionics*, 168 (2004) 51.
14. T. Jiang, S. Zhang, X. Qiu,W. Zhu and L. Chen, *J. Power Sources*, 166 (2007) 503.
15. T. Jiang, S. Zhang, X. Qiu,W. Zhu and L. Chen, *Electrochem. Commun.*, 9 (2007) 930.
16. A. S. Aricò, P. Bruce, B. Scrosati and J. M. Tarascon, *Nat. Mater.*, 4 (2005) 366.
17. L. Bazin, S. Mitra, P. L. Taberna, M. Gressier, M. J. Menu, A. Barnabé, P. Simon and J. M. Tarascon, *J. Power Sources*, 188 (2009) 578.
18. S. H. Ju, H. C. Jang and Y. C. Kang, *J. Power Sources*, 189 (2009) 163.
19. W. Pu, X. He, J. Ren, C. Wan and C. Jiang, *Electrochim. Acta*, 50 (2005) 4140.
20. H. Guo, S. Zhao, H. Zhao and Y. Chen, *Electrochim. Acta*, 54 (2009) 4040.
21. P. A. Connor and J. T. S. Irvine, *Electrochim. Acta*, 47 (2002) 2885.
22. M. Martos, J. Morales and L. Sánchez, *Electrochim. Acta*, 46 (2000) 83.
23. G. X. Wang, J. Yao, H. K. Liu, S. X. Dou and J. Ahn, *Electrochim. Acta*, 50 (2004) 517.
24. N. Tamura, R. Ohshita, M. Fujimoto, S. Fujitani, M. Kamino and I. Yonezu, *J. Power Sources*, 107 (2002) 48.
25. C. Arbizzani, S. Beninati, M. Lazzari and M. Mastragostino, *J. Power Sources*, 141 (2005) 149.
26. M. Yoshio, T. Tsumura and N. Dimov, *J. Power Sources*, 146 (2005) 10.
27. J. Y. Xiang, J. P. Tu, X. L.Wang, X. H. Huang, Y. F. Yuan, X. H. Xia and Z. Y. Zeng, *J. Power Sources*, 185 (2008) 519.
28. L. Huang, H. B.Wei, F. S. Ke, X. Y. Fan, J. T. Li and S. G. Sun, *Electrochim. Acta*, 54 (2009) 2693.
29. G. J. Davies and S. Zhen, *J. Mater. Sci.*, 18 (1983) 1899.
30. G. C. Bond and D. T. Thompson, *Catal. Rev.*, 41 (1999) 319.
31. T. You, O. Niwa, M. Tomita and S. Hirono, *Anal. Chem.*, 75 (2003) 2080.
32. J. R. Weissmueller, N. Viswanath, D. Kramer, P. Zimmer, R. Wuerschum and H. Gleiter, *Science*, 300 (2003) 312.
33. S. H. Joo, S. J. Choi, K. J. Kwa and Z. Liu, *Nature*, 412 (2001) 169.
34. J. Erlebacher, M. J. Aziz, A. Karma, N. Dimitrov and K. Sieradzki, *Nature*, 410 (2001) 450.
35. W. B. Liu, S. C. Zhang, N. Li, J. W. Zheng and Y. L. Xing, *J. Electrochem. Soc.*, 157 (2010) D666.
36. Z. H. Zhang, Y. Wang, Z. Qi, J. K. Lin and X. F. Bian, *J. Phys. Chem. C*, 113 (2009) 1308.
37. W. B. Liu, S. C. Zhang, N. Li, J. W. Zheng, S. S. An and Y. L. Xing, *Int. J. Electrochem. Sci.*, 7 (2012) 6365.
38. Z. Qi, C. C. Zhao, X. G. Wang, J. K. Lin, W. Shao, Z. H. Zhang and X. F. Bian, *J. Phys. Chem. C*, 113 (2009) 6694.
39. W. B. Liu, S. C. Zhang, N. Li, J. W. Zheng and Y. L. Xing, *Microporous Mesoporous Mater.*, 138 (2011) 1.
40. Z. H. Zhang, Y. Wang, Y. Z. Wang, X. G. Wang, Z. Qi, H. Ji and C. C. Zhao, *Scripta Mater.*, 62 (2010) 137.
41. W. B. Liu, S. C. Zhang, N. Li, J. W. Zheng and Y. L. Xing, *Corrosion Sci.*, 53 (2011) 809.
42. W. B. Liu, S. C. Zhang, N. Li, J. W. Zheng, S. S. An and Y. L. Xing, *Int. J. Electrochem. Sci.*, 7

(2012) 2240.
43. Y. Ding and J. Erlebacher, *J. Am. Chem. Soc.*, 125 (2003) 7772.
44. W. B. Liu, S. C. Zhang, N. Li, J. W. Zheng, S. S. An and Y. L. Xing, *Corrosion Sci.*, 58 (2012) 133.
45. Y. Ding, Y. J. Kim and J. Erlebacher, *Adv. Mater.*, 16 (2004) 1897.
46. W. B. Liu, S. C. Zhang, N. Li, J. W. Zheng and Y. L. Xing, *Int. J. Electrochem. Sci.*, 6 (2011) 5445.
47. L. H. Qian and M. W. Chen, *Appl. Phys. Lett.*, 91 (2007) 083105.
48. W. B. Liu, S. C. Zhang, N. Li, J. W. Zheng, S. S. An and G. X. Li, *Int. J. Electrochem. Sci.*, 7 (2012) 7993.
49. W. B. Liu, S. C. Zhang, N. Li, J. W. Zheng and Y. L. Xing, *J. Electrochem. Soc.*, 158 (2011) D611.
50. Y. Ding, A. Mathur, M. W. Chen and J. Erlebacher, *Angew. Chem., Int. Ed.*, 44 (2005) 4002.
51. W. B. Liu, S. C. Zhang, N. Li, S. S. An and J. W. Zheng, *Int. J. Electrochem. Sci.*, 7 (2012) 9707.
52. J. Erlebacher, *J. Electrochem. Soc.*, 151 (2004) C614.
53. W. B. Liu, S. C. Zhang, N. Li, J. W. Zheng and Y. L. Xing, *J. Mater. Sci. Technol.*, 28 (2012) 693.
54. W. B. Liu, S. C. Zhang, N. Li, J. W. Zheng and Y. L. Xing, *J. Electrochem. Soc.*, 158 (2011) D91.
55. A. M. Hodge, J. Biener, J. R. Hayes, P. M. Bythrow, C. A. Volkert and A. V. Hamza, *Acta Mater.*, 55 (2007) 1343.
56. M. Inaba, T. Uno and A. Tasaka, *J. Power Sources*, 146 (2005) 473.
57. S. D. Beattie, T. Hatchard, A. Bonakdarpour, K. C. Hewitt and J. R. Dahn, *J. Electrochem. Soc.*, 150 (2003) A701.
58. R. A. Huggins, *J. Power Sources*, 13 (1999) 81.
59. W. B. Liu, S. C. Zhang, N. Li, S. S. An and J. W. Zheng, *Int. J. Electrochem. Sci.*, 8 (2013) 347.
60. J. C. Lytle, H. Yan, N. S. Ergang, W. H. Smyrl, A. Stein, *J. Mater. Chem.*, 14 (2004) 1616.